Study of the Indoor Millimeter Wavelength Channel

Jung Ryu, Andrzej Partyka, Sundar Subramanian, Ashwin Sampath
Qualcomm CR&D

***Abstract*—In this paper, we conduct ray-tracing simulation studies using WinProp tool to understand the path loss, coverage area, diversity and delay spread of the 29GHz band in the indoor propagation environment, and compare the 29GHz indoor channel to the 2.9GHz indoor channel. In addition, we compare our simulation results with the measurement data from [4].**

Based on our simulation results, we conclude that the 29GHz band has similar indoor channel characteristics as 2.9GHz and that any inherent impairment of the mmWave due to higher carrier frequency can easily compensated with beam forming techniques and other advanced algorithms. Specifically, our results show that the path loss exponents and the RMS delay spread values are similar at 29GHz and at 2.9GHz. In addition, our simulation results show that by having multiple access points on an office floor, we can significantly improve important diversity metrics such as the number of detectable beams and the angular separation of those beams, so as to make 29GHz system using beam forming technique more robust against beam blockage.

I. Introduction

There has been an increased growth in indoor data consumption over the past decade in both enterprise and residential scenarios. Applications like on-demand HD video, instantaneous cloud sync, HQ video chats etc. all increase the demand for very high throughput links in indoor scenarios. In enterprise scenarios, there is also an additional need for always on data and connectivity to the cloud while being not tethered to the Ethernet. While a natural approach is to install more small-cells or APs, the performance does not linearly increase with the increased number of base stations due to the inter base-station interference. There have been a few MIMO approaches that have been suggested to manage this interference, but the gains are not very significant.

Recently, there has been a lot of development and activity on using the millimeter wave (MMW) bands for data access to smart devices. The promise of much larger bandwidths (1.3 GHz at 28 GHz band, 1.4 GHz at 39 GHz band and over 7 GHz at 60 GHz band) have led to many considering these MMW bands to support the very high demand indoor and outdoor use cases such as video streaming. A key benefit is that the beamforming that is possible at these high frequencies also inherently reduces the inter-base station interference and allows for much better spatial reuse.

While the device complexity and cost are some of the main concerns with the use of the MMW band, the primary concern is indeed the propagation of EM waves at these frequencies. The wireless propagation is less likely to diffract around obstacles or penetrate through typical indoor materials at these MMW bands as compared to the lower frequencies. In this paper, we consider the ray tracing approach to study the indoor propagation at 29 and 2.9 GHz bands. We model a floor of our office building and simulate the wireless propagation through ray tracing. The modeling includes the main structural components but does not model the small objects, furniture and people. We generate the coverage and channel statistics results and finally compare them with actual measurements in the same office floor as [4]. Our main contributions are as follows:

A. Main Contributions

1) Our simulation results indicate that in the indoor channel, the path loss of 29GHz mmWave signal and that of 2.9GHz signal are similar and the higher path loss of 29GHz signal can easily be compensated by using more antennas and beam forming at 29GHz carrier frequency. The path loss exponents are 2.9 and 3.0 for 2.9GHz and 29GHz, respectively, for short Tx-Rx separation distances ($< 10m$), and 5.8 and 6.2 for longer Tx-Rx separation distances ($> 10m$).
2) In addition, delay spread is also similar for 29GHz and for 2.9GHz (around 10ns for both), implying the coherence bandwidth characteristic is similar for two bands.
3) Our results also show that by placing multiple access points, the number of beams can be increased by factor of four on the median, and the angular separation between beams can be increased by 25° on the median.

II. Related Work

Measurement results of the indoor 60GHz channel are reported in [9], [11], [6]. [9] was able to match the received beams with propagation paths, showing that ray-tracing can be used to predict the angle of arrival and the power of the received beams. [11] reports that the RMS delay spread is of the same order as we report in this work, and that 60 GHz system can still work in many cases, when the strongest path is blocked. [6] report that the 60GHz channel between transmitter and receiver consists mostly of the LOS path and the signal paths of the first and second order reflections, and that the transmitter and the receiver antennas must be correctly polarized to maintain a good link. In addition, [5], [7] studied the reflection and transmission properties of indoor building materials that are useful in building the indoor simulation environment.

[3], [4] contain results of indoor 28/29GHz measurement campaigns. The path loss exponents reported in [3] (1.43 for LOS and 2.68 for NLOS) are substantially different from here and in [4]; the indoor measurements in [3] are done over multiple floors in a shopping mall like environment. However, RMS delay and angular spread as reported in [3] are similar to our values. [8], [10], [2] discuss outdoor 28GHz channel environment. The discrepancy between measured RMS delay spread [8], [2] and the simulated RMS delay spread [10]

978-1-4799-5952-5/15/$31.00 ©2015 IEEE

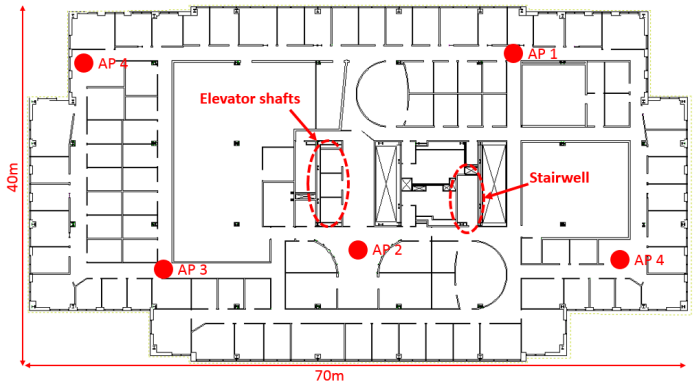

Fig. 1. Map of the simulated indoor floor. The locations of access points are indicated with red dots.

is similar to the discrepancy between the measured and the simulated we report in this paper - the measured indoor RMS delay is much larger than the simulated; the difference between simulated RMS delay and measured RMS delay suggests that it is difficult to predict the RMS delay through simulations, likely because simulation can not model all the small objects found in the real world that become more reflective at high carrier frequency.

III. Coverage and Path Loss Results

WinProp channel simulation was performed on the fourth floor of our corporate building, which is a typical corporate office space as shown in Figure 1. The office environment mostly consists of office rooms and conference rooms. We study the channel both at 29GHz and at 2.9GHz. The path loss was computed using omni-directional antennas both at the transmitter and receiver, and we have measurement data from [4] with which we can compare our simulated path loss data. We simulate the case where we have a single access point and multiple access points spread through the floor. The access points are set at the height of 2.5m and the UE/receiver locations are set at the height of 1.5m. The relative dielectric constants used in the simulations are 4 for wall, 5 for glass and 1.7 for wood. The inner walls are made of two layers of material of total thickness of 15cm. We only model building structures such as walls, columns, stairs and elevator shafts; humans and furniture and other non-structural objects are not modeled. Details of how WinProp simulates reflections, diffractions, and scattering can be found in [1].

The simulated path loss data at 29GHz and 2.9GHz are shown in Figures 2 and 3 (with only AP 1 active). The path loss shown in the figures is in reference to path loss at $d_0 = 1m$ Tx-Rx separation distance. The path loss at $1m$ distance is 41.7dB at 2.9GHz and 61.7dB at 29GHz. [4] uses the following two piece-wise linear log-linear models to model the path loss vs. distance relationship. For distances $d < d_t = 10m$, the sample data is fit to the following log-linear model:

$$PL(d)_{[dB]} = PL(d_0)_{[dB]} + \beta 10\log_{10}(d/d_0) + X \quad (1)$$

where X is a random variable with normal distribution $\mathcal{N}(0, \sigma^2)$. For distances $d \geq d_t = 10m$, the following log-linear model is used to fit the sample data:

$$PL_1(d)_{[dB]} = PL(d_t)_{[dB]} + \beta_1 10\log_{10}(d/d_t) + X_1 \quad (2)$$

	Simulation Data		Measurement Data	
	2.9GHz	29GHz	2.9GHz	29GHz
β	2.92137	3.01492	2.2	2.6
σ	6.7524	7.1832	1.94	5.75
β_1	5.81307	6.18131	4.9	5.2
σ_1	25.357	24.0624	5.8	7.55

TABLE I. Parameters for the log-linear models in Eqs. (1) and (2) obtained using simulation data in this paper and parameters obtained by [4] using their measurement data.

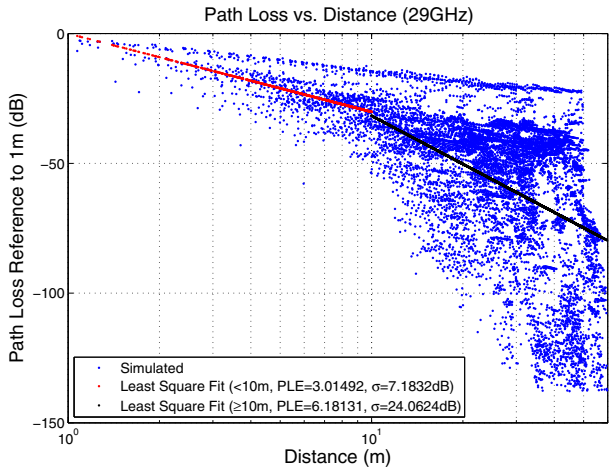

Fig. 2. Simulated path loss at 29GHz. The points corresponding to path loss of -80dB or greater (with reference to 1m) correspond to light green to blue areas in Figure 6.

where X_1 is a random variable with normal distribution $\mathcal{N}(0, \sigma_1^2)$. To make the piece-wise linear models continuous, $PL_1(d_t)_{[dB]} = PL(d_t)_{[dB]}$.

The values we obtain for β, β_1, σ, and σ_1 for 2.9GHz and 29GHz using simulation data are shown in Table I. In addition, we show in Table I the log-linear model parameters that [4] obtained by using their measurement data. The table shows that the log-linear model obtained using our simulation data over estimates the path loss exponent with greater variance (larger σ and σ_2). The standard deviation of the log normal shadowing variable in the path loss plot in Figures 2 and 3 exhibit dependency on the Tx-Rx separation distance. In Figure 4, we plot the standard deviation of the log normal shadowing using a sliding window of 5m vs. Tx-Rx separation distance, and the linear fit of the data using least squares fit; the linear fit indicates that the σ of the log normal shadowing random variable increases linearly with the Tx-Rx distance. For 29GHz, the linear fit is:

$$\sigma(\text{dB}) = 0.5103 \times \text{Tx-Rx Distance (m)} + 6.6318(\text{dB}). \quad (3)$$

For 2.9GHz, the linear fit is:

$$\sigma(\text{dB}) = 0.6417 \times \text{Tx-Rx Distance (m)} + 4.1988(\text{dB}). \quad (4)$$

Figure 5 shows the CDF of received signal power at 29GHz with AP 1 active and with all AP's active. The received signal power is computed using omni-directional transmit and receive antennas. Figures 6 and 7 show the map of the received signal power on the simulated map. Note that when all AP's are active, the receiver would connect to the AP with the strongest received signal, and because of this, the received power when

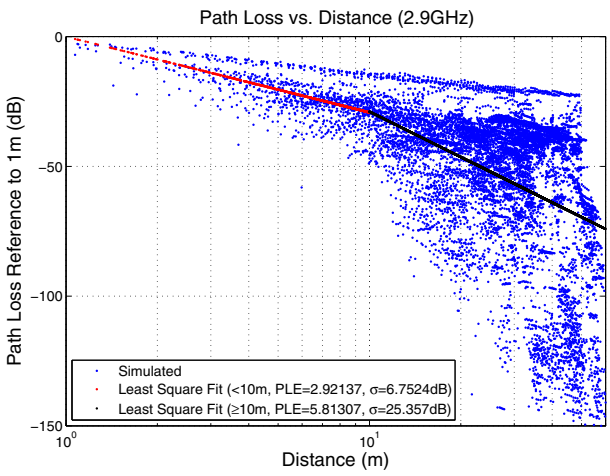

Fig. 3. Simulated path loss at 2.9GHz.

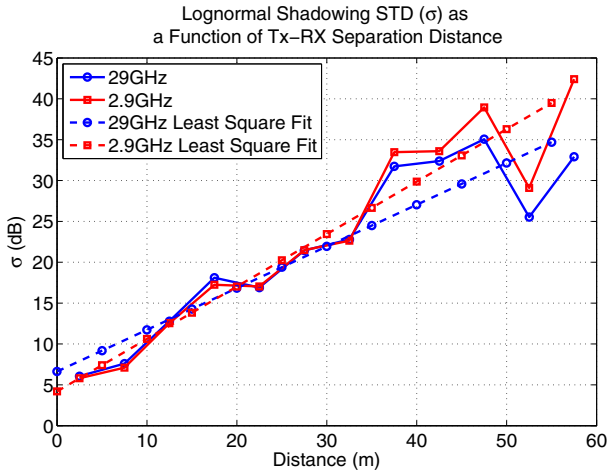

Fig. 4. Standard deviation of the log normal shadowing random variable (X in Eqs. 1 and 2) using a sliding window of 5m vs. Tx-Rx separation distance, and the linear fit of the data using least squares fit.

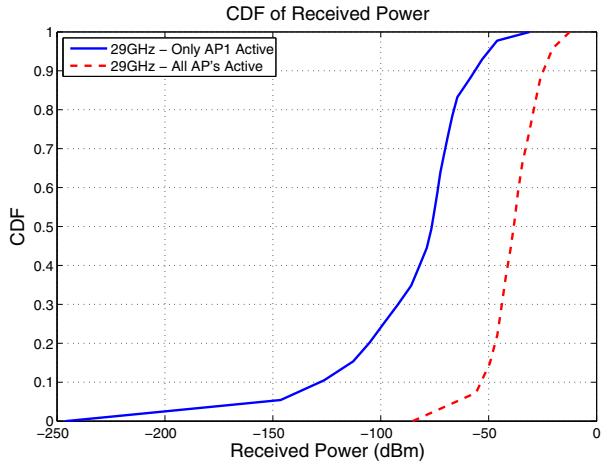

Fig. 5. Received signal power collected with omni-directional antenna when only AP 1 is active and with all AP's active. Note that when all AP's are active, the receiver would connect to the AP with the strongest received signal, and because of this, the received power when all AP's are active is about 40dB greater than when only AP 1 is active on the median.

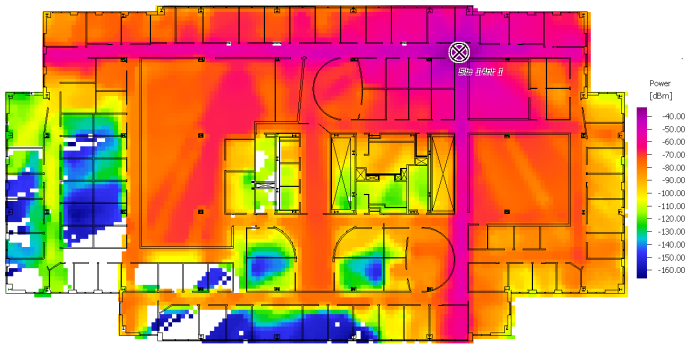

Fig. 6. Received power map of 29GHz when only AP 1 is active.

Fig. 7. Received power map of 29GHz when all AP's are active. Red: power<-90dBm, yellow: -90dBm≤power<-80dBm, green: -80dBm≤ power <-70dBm, blue: -70dBm≤ power <-60dBm, magenta: -60dBm≤power.

all AP's are active is about 40dB greater than when only AP 1 is active on the median.

IV. Beam Diversity

The short wavelength of 29GHz allows transmit and receive beam forming techniques to be used to improve the received signal quality. Beam forming concentrates the signal energy onto a particular propagation path; however, if the propagation path gets blocked by an object, the transmitter and the receiver must switch to a different propagation path to maintain the link. Hence, the availability and the quality of a secondary propagation path/beam are important properties to consider for 29GHz system. In this section, we study the number of useful clusters (beams) and the quality of those beams (power and angular separations) at 29GHz with single AP and with multiple AP's. Our minimum target is to support 200Mbps or higher in the 500MHz bandwidth at 29GHz; we assume that a practical indoor 29GHz system would be equipped as shown in the link budget Table II. Hence, using the table, we calculate that our maximum target path loss of 143dB.

A. Cluster Count

Figure 8 shows the CDF of the number of clusters/beams seen by a receiver with the access point 1 or with all access points active at 29GHz. For when only one access point is active, two beams are considered distinct if their angular separation is 10° or more, either in azimuth or elevation, and the beam power is such that the path loss is at maximum 143dB.

Operating Frequency (GHz)	29
Transmitter Parameters	
Total Tx Power (dBm)	25
Number of Antennas	32 (16 × 2 planar array)
Array Gain (dB)	15.05
Per Elem. Antenna Gain (dB)	15
Total Antenna Array Inefficiency Loss (dB)	3
Net Transmit Antenna Array Gain (dB)	27.05
Total EIRP (dBm)	52.05
dBm per Element	9.95
Receiver Parameters	
Total Operating Bandwidth (MHz)	500
Noise Figure (dB)	11
Thermal Noise Power (dBm)	-87
Receive Antenna Gain (dB)	15
Rx Digital Inefficiency (dB)	5
Target Operating SNR (dB)	-5
Target Effective Data Rate (Mbps)	198.20
Maximum Supportable Pathloss(dB)	143.05

TABLE II. LINK BUDGET PARAMETERS - THE MAXIMUM PATH LOSS IS 143.05 DB IN ORDER TO SUPPORT 200MBPS OR HIGHER.

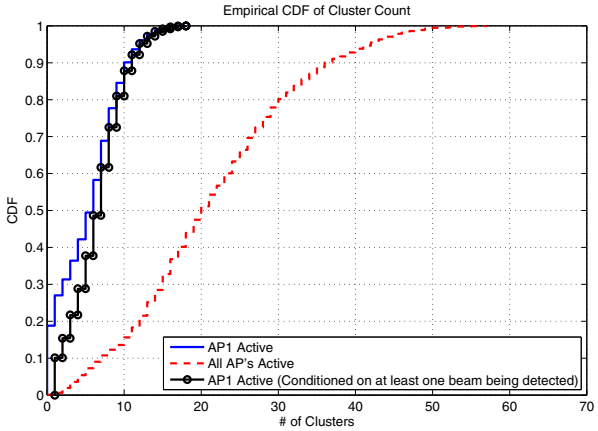

Fig. 8. CDF of the number of clusters seen by a receiver with either access point 1 or with all access points active.

When all access points are active, the receiver considers two beams to be distinct if the beams are separated by at least 10°, either in azimuth or elevation, with path loss of at most 143dB, regardless of which access points the beams come from. Figure 9 shows the number of beams detected by the UE when only access point 1 is active, and Figure 10 shows the number of beams seen at various locations when all access points are active. The figures show that the number of beams seen by a receiver can be increased by a factor of five on median by having a reasonable number of access points placed on an office floor.

B. Beam Power

Figure 11 shows the CDF of the received power of the strongest beam the UE would detect when only access point 1 is active or when all access points are active. The figure shows that on median, there is 20dB increase in the strongest beam power when all access points are active. In Figure 12, we plot the CDF of the power fraction of the second strongest beam

Fig. 9. Map of the number of clusters seen by a receiver in the vicinity of access point 1. Green: 1 or 2, yellow: between 3 and 7, blue: between 8 and 12, and red: 13 or more beams. White space = no detectable beams.

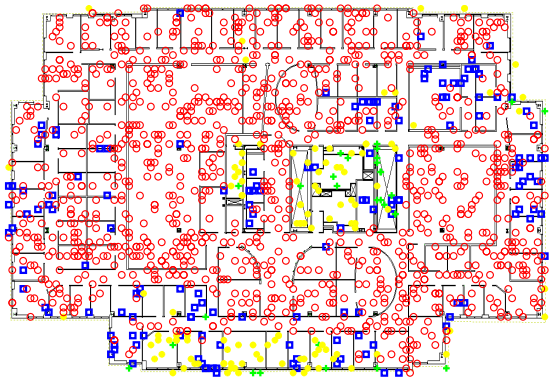

Fig. 10. Map of cluster count with all access points active. Green '+': 2 or fewer beams, yellow '*': between 3 and 7, blue squares: between 8 and 12, and red 'o': 13 or more beams.

to the most strongest beam. We define the power fraction as

$$\frac{\text{RX power of } 2^{\text{nd}}\text{strongest beam}}{\text{Sum RX power of } 1^{\text{st}} \text{ and } 2^{\text{nd}} \text{ strongest beams}}.$$

We see that the power fraction does not change with the increase in the number of active access points.

C. Angle of Arrival

Figure 13 shows the CDF of the angle of arrival (AOA) angular difference between the strongest and the second strongest beams, with one access point or with all access points active. Larger angular separation is desirable since this would make having two beams blocked at the same time less likely. The figure shows that by increasing the number of active access points, the angular difference between the strongest and the second strongest beams increases by about 24° for 29GHz system.

D. Comparison against Measurement

Lastly, we compare our simulation results with results from spherical scan measurements at 29GHz of the indoor

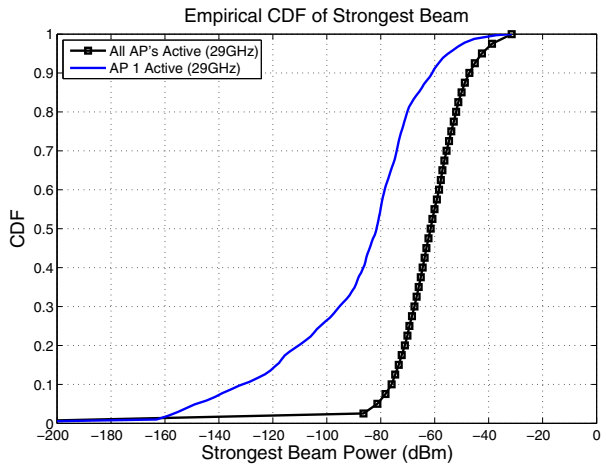

Fig. 11. CDF of the strongest beam from access point 1 alone or from any one of the five access points.

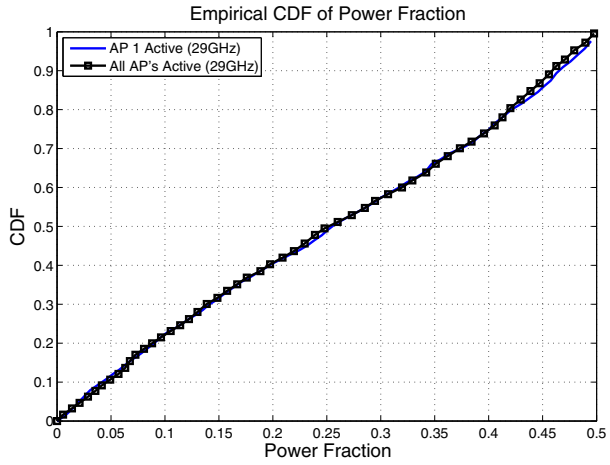

Fig. 12. CDF of the second strongest beam as fraction of the combined powers of the strongest and the second strongest beams.

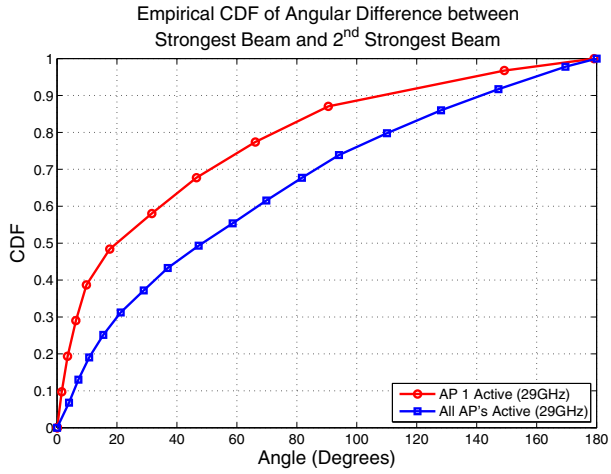

Fig. 13. CDF of angular difference between strongest and second strongest beams

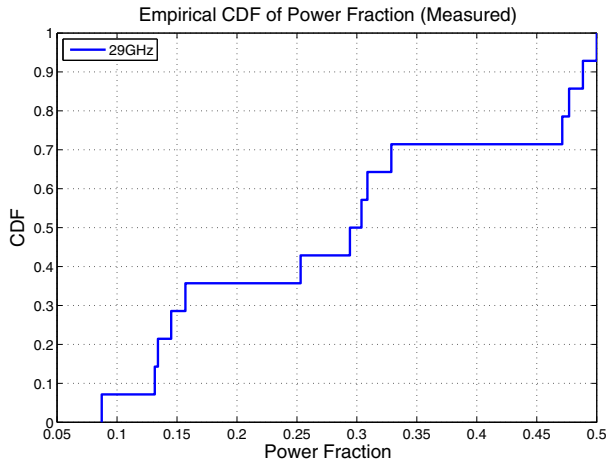

Fig. 14. CDF of the second strongest measured beam as fraction of the combined powers of the strongest and the second strongest measured beams. Measurement results taken from [4].

channel from [4]. The measurement campaign in [4] used one channel sounding transmitter and used one receiver to measure the channel at various locations on the map shown in Figure 1. We obtained 14 spherical scan measurements in [4] and analyzed the results to obtain the cluster counts, power fraction of the strongest and the second strongest beams and the angular separations between them. Out of the 14 scans, 6 scans had exactly two beams/clusters (43%) and the rest had 3 or more beams. Comparing against the conditional CDF of the cluster count when only one AP is active in Figure 8, we see that our simulation over predicts the cluster count. Figure 14 shows the CDF of the second strongest measured beam as fraction of the combined powers of the strongest and the second strongest measured beams; compare the measurement results with the CDF shown in Figure 12, and note that on median, the second strongest beam is 0.25 of the combined power in simulations and 0.3 in measurements. Figure 15 shows the measured angular difference between the strongest and the second strongest beams. In conclusion, the simulation predicts more beams that are closer, but measurement results show fewer beams that are spaced farther apart.

V. Delay Spread

Figure 16 shows the CDF of RMS delay spread at 2.9GHz and 29GHz with either access point 1 or all access points active. The RMS delay is computed with omni-directional transmit and receive antennas. The plot shows that the RMS delay spread is less than 10ns on median for both 2.9GHz and 29GHz. The map in Figure 17 shows the RMS delay values at various receiver locations when all AP's are active. Our simulation data shows that RMS delays are about the same on median for both 29GHz and 2.9GHz. The measured RMS delay spread (measured with omni-directional antennas) from [4] for 29GHz is about on average 10% smaller than at 2.9GHz, as shown in Table III and included here for comparison purposes. The measurement data shows that RMS delay is about 3 to 5 times larger than the simulated RMS delay values. The discrepancy between simulation data here and measurement data from [4] is consistent with the discrepancy between outdoor simulation data in [10] and outdoor

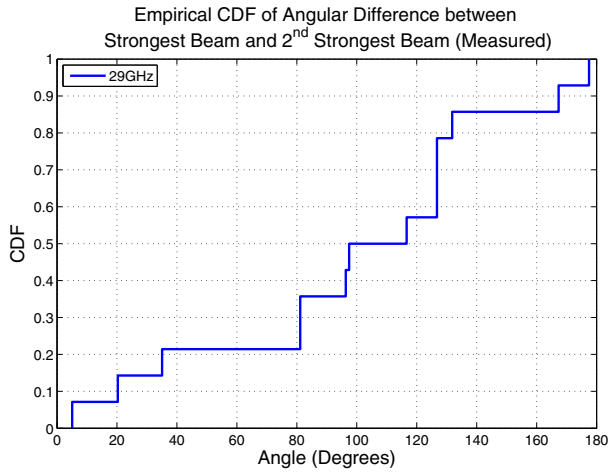

Fig. 15. CDF of the measured angular difference between the strongest and the second strongest beams. Measurement results taken from [4].

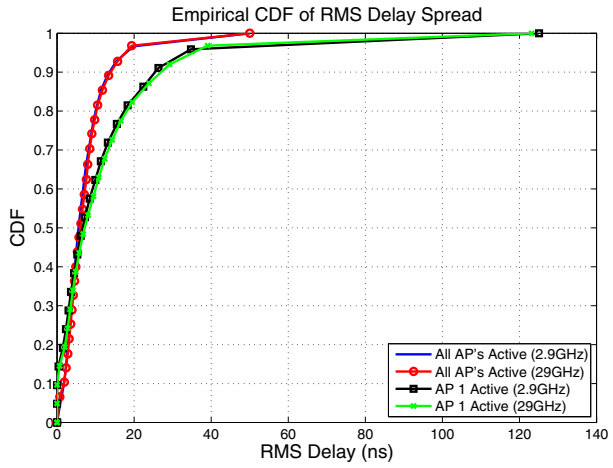

Fig. 16. CDF of RMS delay. The CDF shows that on median, RMS delay is less than 10ns in indoors.

measurement data in [2] in that measurement data shows much larger delay spread; the possible reason for discrepancy could be that real channel environment contains many more reflective and scattering small objects that our simulation model can not model.

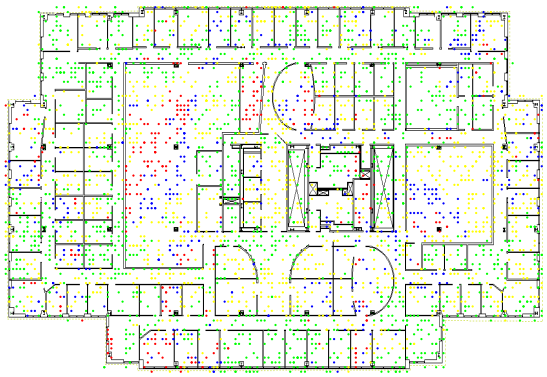

Fig. 17. RMS delay for 29GHz at various receiver locations with all access points active. Green: less than 5ns, yellow: between 5ns and 10ns, blue: between 10ns and 15ns, and red: greater than 15ns.

Tx 460J		
Rx Location	2.9GHz	29GHz
430D	43.1	32.1
430J	52.2	34.9
430B	45.9	49.4
430N	37.75	34.5
430Q	39.6	37.9
415P	43.7	39.8
415K	34.9	21.1
440C	47.3	60.4
FIRE EXT	54.5	53.7
415I	31.7	38.1
440G	43.1	39.9
440I	33.3	42.3
415H	36.1	20.7
420_2	55.5	43.7
SUITE 415	60.8	53.9
420_3	56.7	47.5
415G	31.3	37
420_BACK	58.7	49

TABLE III. MEASURED RMS DELAY SPREAD AT 29GHZ. THE TABLE SHOWS THAT THE RMS DELAY SPREAD AT 29GHZ (AVERAGE 40.88NS) IS ABOUT 10% SMALLER THAN THAT AT 2.9GHZ (AVERAGE 44.78NS).

REFERENCES

[1] WinProp User Manual. http://www.awe-communications.com.

[2] M. R. Akdeniz, Y. Liu, S. Sun, S. Rangan, T. S. Rappaport, and E. Erkip. Millimeter wave channel modeling and cellular capacity evaluation. *arXiv preprint arXiv:1312.4921*, 2013.

[3] S. Hur, Y. Cho, K. Lee, J. Ko, and J. Park. Millimeter-wave channel modeling based on measurements in building and campus environments at 28GHz. In *EURO-COST*, 2014.

[4] O. Koymen, A. Partyka, S. Subramanian, and J. Li. Indoor mm-Wave channel measurements: Comparative study of 2.9 GHz and 29 GHz. In *EURO-COST*, 2014.

[5] B. Langen, G. Lober, and W. Herzig. Reflection and transmission behaviour of building materials at 60GHz. In *Fifth IEEE International Symposium on Personal, Indoor and Mobile Radio Communications*, 1994.

[6] A. Maltsev, R. Maslennikov, A. Sevastyanov, A. Khoryaev, and A. Lomayev. Experimental investigations of 60GHz wlan systems in office environment. In *IEEE Journal on Selected Areas in Communications*, 2009.

[7] K. Sato, T. Manabe, T. Ihara, H. Saito, S. Ito, T. Tanaka, K. Sugai, N. Ohmi, Y. Murakami, M. Shibayama, Y. Konishi, and T. Kimura. Measurements of reflection and transmission characteristics of interior structures of office building in the 60-GHz band. In *IEEE Transactions on Antennas and Propagation*, 1997.

[8] A. I. Sulyman, A. T. Nassar, M. K. Samimi, G. R. MacCartney, T. S. Rappaport, and A. Alsanie. Radio propagation path loss models for 5g cellular networks in the 28GHz and 38GHz millimeter-wave bands. In *IEEE Communications Magazine*, 2014.

[9] H. Xu, V. Kukshya, and T. S. Rappaport. Spatial and temporal characteristics of 60GHz indoor channels. In *IEEE Journal on Selected Areas in Communications*, 2002.

[10] Z. Zhang, J. Ryu, S. Subramanian, and A. Sampath. Coverage and channel characteristics of millimeter wave band using ray tracing. In *IEEE ICC*, 2015.

[11] T. Zwick, T. Beukema, and H. Nam. Wideband channel sounder with measurements and model for the 60 GHz indoor radio channel. *Vehicular Technology, IEEE Transactions on*, 54(4):1266–1277, July 2005.